https://doi.org/10.5194/egusphere-2026-1016
Preprint. Discussion started: 19 March 2026

Spatio-Temporal Non-Stationarity of Flood Risk in the European Alps over the last 1,450 Years

Hansjörg Albrecher[1,2], Maria Laura Battagliola[3], Martin Bladt[4], Alaric J.A. Müller[1], and Tina Swierczynsk[5]

[1]Department of Actuarial Science, Faculty of Business and Economics, University of Lausanne, UNIL-Chamberonne, CH-1015 Lausanne Switzerland
[2]Swiss Finance Institute and Expertise Center for Climate Extremes (ECCE), Lausanne CH-1015, Switzerland
[3]Department of Statistics, Instituto Tecnológico Autónomo de México, Río Hondo 1, Altavista, Álvaro Obregón, 01080 Ciudad de México, CDMX, Mexico
[4]Department of Mathematical Sciences, University of Copenhagen, Universitetsparken 5, DK-2100 Copenhagen, Denmark
[5]GFZ German Research Centre for Geosciences, Telegrafenberg, GE-14473 Potsdam, Germany

Correspondence: Maria Laura Battagliola (laura.battagliola@itam.mx)

Abstract. Floods are a major source of losses from natural hazards, yet modelling their occurrence and severity is challenging due to complex spatial dependencies and non-stationary behaviour over time, both of which are increasingly affected by climate change. In this study, we characterise spatial and temporal non-stationarity in flood risk and quantify the dependence of flood occurrences under minimal modelling assumptions. We analyse a unique dataset of flood records from 27 Alpine lakes spanning 1,450 years, applying penalised additive mixed models to capture the empirical spatio-temporal dependence structure of flood events. Our results reveal pronounced regional and temporal variations in flood risk and highlight periods of elevated susceptibility. The model further allows extrapolation of flood occurrence probabilities to unobserved locations across the European Alps, providing a robust tool for hazard assessment under changing climatic conditions.

1 Introduction

Floods are a major source of economic losses due to natural catastrophes. In 2021 alone, they caused USD 80 billion in damages, of which USD 20 billion were insured, and globally, insured losses due to floods over the last 20 years have accumulated to USD 140 billion (Bevere and Remondi, 2022). Given the magnitude of catastrophic flood events, understanding their underlying mechanisms and occurrence patterns is crucial both for enhancing the resilience of affected communities and for (re)insurance companies in order to provide appropriate coverage.

Despite the increasing frequency of extreme weather events, the long-term variability of flood occurrences in the European Alps remains only partially understood. Most studies rely on short-term hydrometric records, which often fail to capture variability over centuries or millennia. Due to the complex interplay between climatic and geomorphological factors, statistical methods that can analyse flood patterns across space and long temporal scales are powerful tools to better understand past flood regimes and to inform future hazard assessments.

https://doi.org/10.5194/egusphere-2026-1016
Preprint. Discussion started: 19 March 2026

Several approaches have been used to investigate flood occurrence patterns. Using hydrometric records, Merz et al. (2016) analysed 80 years of flood data across Germany to determine whether significant changes of flood occurrence patterns throughout time are present. Their results suggest that temporal clustering depends on the considered flood severity and time scale. In a pan-European database covering more than 4000 hydrometric stations over the last five decades, Blöschl et al. (2017) detected significant changes in the timing of floods within a year, which can be interpreted as a climate signal at the continental scale. Expanding the scope further, Blöschl et al. (2019) observed considerable regional differences in whether climate change increases or decreases river flood frequency, highlighting the heterogeneous nature of flood responses to climate forcing.

An alternative approach relies on lake sediment data, which provide long-term flood reconstructions beyond the limits of hydrometric records. During floods, soil erosion in the lake's watershed transports sediments to the lake through runoff and river flow. The deposition of these sediments forms distinct flood layers within the lake sediments, which can be attributed to specific years, allowing the reconstruction of flood histories spanning up to 10,000 years (Wilhelm et al., 2019, Sec.2.4). For example, Swierczynski et al. (2013) investigated the variation of flood frequency around Lake Mondsee (Austria) over the last 7,100 years, analysing regional and seasonal features of flood occurrence under changing climate conditions. Similar studies have been conducted for lakes in England (Chiverrell et al., 2019) and Norway (Engeland et al., 2020). Building on these efforts, Wilhelm et al. (2022) compiled the largest currently available paleo-flood dataset, comprising 27 lakes in the European Alps with records ranging from 150 to 10,000 years, and applied a statistical study of marginal flood frequency to each site.

In this paper, we extend the analysis presented in Wilhelm et al. (2022) by employing Generalised Additive Models (GAMs), a flexible statistical framework that allows data-driven non-linear relationships between predictors and response variables without enforcing their shape (Hastie and Tibshirani, 1986; Wood, 2017). GAMs provide a balance between interpretability and predictive accuracy, making them particularly useful for paleoflood records where abrupt shifts in flood frequency may occur over different climatic regions or periods. Furthermore, GAMs can be extended to Generalised Additive Mixed Models (GAMMs), which can be used to incorporate spatially and temporally structured dependencies. This is crucial for paleo-sediment data, as flood records are often irregularly distributed in space and time. Spatial smoothing and hierarchical modelling within GAMMs help interpolate missing data and provide robust estimates of flood probability, even in locations with limited direct observations. This methodology allows for a detailed reconstruction of past flood regimes and lays the groundwork for more reliable predictions under future climate scenarios.

Various fields have benefitted from the application of GAMs, including hydrology and flood risk. Chebana et al. (2014) introduced GAMs in regional flood frequency analysis (RFFA) for 151 hydrometric stations in Québec, Canada, highlighting the limitations of traditional log-linear regression models in capturing non-linear relationships between flood quantiles and basin characteristics. Similarly, Rahman et al. (2018); Rima et al. (2025) applied GAMs for RFFA in Australia, demonstrating that GAMs provide more accurate and reliable estimates of flood quantiles compared to less flexible methods. In the context of Alpine hydrology, Brunner and Naveau (2023) used GAMs to reconstruct reservoir operation signals for 74 central Alpine catchments, predicting natural streamflow conditional on covariates such as temperature, precipitation, day of the year, and glacier mass balance changes, and identifying distinct reservoir management strategies, including pronounced seasonal water redistribution in high-elevation catchments.

https://doi.org/10.5194/egusphere-2026-1016
Preprint. Discussion started: 19 March 2026

Our dataset consists of flood records from 27 Alpine lakes, dating back up to 9,050 years. For each lake, we know whether a flood occurred in any given year and we have spatial information, including latitude, longitude, altitude, and catchment area. Our objective is to analyse the evolution of yearly flood probabilities over time while considering the spatial characteristics of each location. GAMs and GAMMs are particularly suited to this task: they allow modelling of flood occurrence likelihood as a smooth function of space and time, include random effects to capture spatial correlation, and can accommodate hierarchical structures inherent in repeated or grouped observations (Wood, 2006, 2017). The inclusion of covariates allows flexible assessment of non-linear effects, confirming or refuting their relevance for lake sediment flood data. Additive models also naturally handle missing observations due to the continuous nature of the estimated effects, enabling robust reconstruction across irregular temporal records. The resulting model can therefore be interpreted as a continuous-time and continuous-space interpolation of discrete flood events, providing a comprehensive estimate of flood probability over the Alpine region.

The remainder of this paper is organised as follows. Section 2 provides the theoretical foundations of the Generalised Additive Mixed Model framework, detailing the mathematical advantages of penalised splines and random effects for hazard modelling. In Section 3, we describe the study area and the paleoflood dataset from the 27 Alpine lakes. Section 4 presents the spatio-temporal model specification, where we justify the treatment of flood occurrences as increments of a counting process to ensure statistical robustness. The empirical results, including the reconstruction of flood probabilities over the last 1,450 years and the identification of significant spatial and temporal predictors, are presented in Section 5. These findings are further interpreted and contextualised in the conclusion, where we discuss the physical implications of the identified trends in relation to climatic variability and conclude with an outlook on the potential applications of this framework for quantitative flood risk assessment and (re)insurance strategies.

2 The Generalised Additive Mixed Model framework

We slightly adapt the notation from Wood (2006, 2017). Let $\{Y_s(t) : t \in \mathcal{T}, s \in \mathcal{S}\}$ denote a (for our purposes one-dimensional) stochastic process defined on the compact spatial set $\mathcal{S} \subset \mathbb{R}^{+,2}$ and a compact temporal domain $\mathcal{T} \subset \mathbb{R}^+$. It is assumed that the random variable $Y_s(t)$, conditionally on the covariate vector $\mathbf{X}_{s,t}$ and for fixed $s \in \mathcal{S}$ and $t \in \mathcal{T}$, follows an exponential family distribution. That is, in a GAMM we have

$$Y_s(t) \mid \mathbf{X}_{s,t} \sim \mathrm{EF}(\mu_s(\mathbf{X}_{s,t}), \phi), \quad s \in \mathcal{S}, t \in \mathcal{T}, \tag{1}$$

where ϕ is the scale parameter and the conditional expectation of the distribution takes the form

$$\mu_s(\mathbf{X}_{s,t}) = \mathbb{E}(Y_s(t) \mid \mathbf{X}_{s,t}) = g^{-1}\left(\mathbf{W}_{s,t}\boldsymbol{\beta} + \mathbf{Z}_s\mathbf{u} + \sum_{i \in \mathcal{I}} f_i(\mathbf{X}^i_{s,t})\right) = g^{-1}(\eta_s(t)). \tag{2}$$

Here, $g(\cdot)$ is a known continuous monotone link function. For each observation (s,t), $\mathbf{W}_{s,t} \in \mathbb{R}^{1\times p}$ denotes a row vector of covariates entering the model linearly with corresponding coefficient vector $\boldsymbol{\beta} \in \mathbb{R}^p$. The term $\mathbf{Z}_s \in \mathbb{R}^{1\times q}$ is a design vector for random effects, and $\mathbf{u} \in \mathbb{R}^q$ is a vector of random effect coefficients with distribution $\mathbf{u} \sim N(0, \boldsymbol{\Psi})$, where $\boldsymbol{\Psi} \in \mathbb{R}^{q\times q}$ is an unknown covariance matrix.

https://doi.org/10.5194/egusphere-2026-1016
Preprint. Discussion started: 19 March 2026

Finally, for a finite set of indices $\mathcal{I}$, $\{f_i(\cdot)\}_{i\in\mathcal{I}}$ are unknown smooth functions that introduce non-linear effects of covariates on the distribution (1). Each function depends on the i-th component $\mathbf{X}^i_{s,t}$ of the covariate vector $\mathbf{X}_{s,t}$. The cardinality of $\mathcal{I}$ is not fixed a priori, as it depends on the number of smooth terms included in the model.

2.1 Smooth function representation

We now go into the details of the additive part of model (2). In order to carry out the estimation for the unknown smooth functions $\{f_i(\cdot)\}_{i\in\mathcal{I}}$, we represent them as a linear combination of known basis functions $\{a_j(\cdot)\}_{j=1,\dots,J}$ with unknown coefficients $\{\alpha_{ij}\}_{i\in\mathcal{I},j=1,\dots,J}$. Let $\mathbf{A}(x) = (a_1(x),\dots,a_J(x))'$. Thus, for each non-linear term, we have

$$f_i(x) = \sum_{j=1}^{J} \alpha_{ij} a_j(x) = \mathbf{A}(x)'\boldsymbol{\alpha}_i, \quad i \in \mathcal{I}. \tag{3}$$

When $f_i(\cdot)$ is evaluated over a finite set of observations $\{x_k\}_{k=1}^n$, the vector of evaluations $(f_i(x_1),\dots,f_i(x_n))'$ can be written in matrix form as $\mathbf{A}\boldsymbol{\alpha}_i$, where $\mathbf{A} \in \mathbb{R}^{n\times J}$ is the corresponding model matrix with rows $\mathbf{A}(x_k)'$, and $\boldsymbol{\alpha}_i' = (\alpha_{i1},\cdots,\alpha_{iJ})$ are the corresponding coefficients. By exploiting (3), smooth predictors of multiple covariates can be constructed as tensor products of marginal smooth basis functions (see Wood (2006)). For example, consider a smooth function $f(\cdot)$ of three covariates x, y, z. Given the sets of marginal basis functions $\{a(\cdot)\}_{j=1}^J, \{b(\cdot)\}_{k=1}^K, \{c(\cdot)\}_{l=1}^L$ chosen for x, y, z, the three-dimensional function can be expressed as

$$f(x,y,z) = \sum_{j=1}^{J}\sum_{k=1}^{K}\sum_{l=1}^{L} \alpha_{jkl} a_j(x) b_k(y) c_l(z). \tag{4}$$

Naturally, formulation (4) can be adapted to deal with any number of covariates. That is, a larger number of covariates can be considered either as additional marginal bases or as multivariate basis functions. For any set of covariate observations, a model matrix $\mathbf{A}_{xyz}$ can be produced from the marginal model matrices $\mathbf{A}_x$,$\mathbf{B}_y$ and $\mathbf{C}_z$. Given the row-wise Kronecker product $\odot$, we have

$$\mathbf{A}_{xyz} = \mathbf{A}_x \odot \mathbf{B}_y \odot \mathbf{C}_z, \tag{5}$$

if the ordering of marginal basis function evaluations is respected. Note that Wood (2017) contains extensive material about the possible basis functions generally used in GAMs.

Having established a finite representation of the non-linear terms $\{f_i(\cdot)\}_{i\in\mathcal{I}}$ using known basis functions, the next step is to prevent overfitting during estimation. Including too many basis functions can result in an overly "wiggly" fit that introduces artifacts, whereas using too few fails to capture the underlying structure of the data. Consequently, it is crucial to find a trade-off, which is achieved by employing a sufficiently large number of basis functions while penalizing their coefficients appropriately. In particular, a quadratic penalty term

$$J_i(f_i) = \boldsymbol{\alpha}_i'\mathbf{P}_i\boldsymbol{\alpha}_i \tag{6}$$

is included when performing estimation. In the present application, the quadratic term is based on the integrated squared curvature, namely the second derivative, of the smooth function. Concretely, $\mathbf{P}_i$ is obtained from integrated squared derivatives

https://doi.org/10.5194/egusphere-2026-1016
Preprint. Discussion started: 19 March 2026

of the basis functions, as in standard spline-based smoothers (see Wood (2017)). There are multiple ways to determine penalties of the form (6), but for the sake of conciseness, we refer readers to Wood (2017) for more details on how such terms are obtained in practice. Moreover, we note penalty terms for multidimensional predictors similarly to (6).

With a slight modification to (6), it is possible to embed in the penalty term a way to shrink the whole function $f_i(\cdot)$ in case it is found to be negligible in the data description. In particular, it suffices to consider

$$J_i(f_i) = \boldsymbol{\alpha}_i' (\mathbf{P}_i + \epsilon_i \mathbf{I}) \boldsymbol{\alpha}_i, \tag{7}$$

with $\boldsymbol{I}$ the identity matrix of appropriate dimension and $\epsilon_i > 0$ a small constant.

2.2 Random effects representation

Random effects in GAMMs allow for the inclusion of hierarchical structures, group-level variations, and dependency structures in the model. Such effects are incorporated through the term $\mathbf{Z}_s\mathbf{u}$ in (2), where $\mathbf{Z}_s$ is a design vector mapping observations to random effect levels, and $\mathbf{u} \sim N(0, \boldsymbol{\Psi})$ is a vector of random effect coefficients with an unknown positive definite covariance matrix $\boldsymbol{\Psi}$.

A simple case is when each spatial location $s \in \mathcal{S}$ belongs to a discrete group (e.g., a region, a station, or a time-based cluster), and the effect of each group is modelled as a random intercept. This assumes that observations within the same group share a common deviation from the overall mean. Concretely, the random intercept model corresponds to

$$\mathbf{Z}_s\mathbf{u} = u_s, \tag{8}$$

where $u_s \sim N(0, \sigma_s^2)$ represents the random effect for group s (location in our case). If the $\{u_s\}_s$ are independent across groups, this formulation introduces intra-group correlation only, meaning that observations from the same location are expected to be more similar than those from different groups.

In the additive models' framework, including GAMM, random effects are estimated with a penalty term, much alike what we described for non-linear terms in the previous section. Specifically, we consider random intercepts (8) with penalty

$$J_{\mathbf{u}} = \mathbf{u}' \boldsymbol{\Psi}^{-1} \mathbf{u},$$

where random effects coefficients are penalized based on their empirical covariance structure $\boldsymbol{\Psi}$. In spatial applications it is common to allow the random intercepts to be correlated as a function of distance, so that observations from nearby locations are also dependent. In that case, given two observations $Y_{s,t}$ and $Y_{s',t'}$, their covariance can be expressed as

$$\mathrm{Cov}(Y_{s,t}, Y_{s',t'}) = \begin{cases} \sigma^2, & \text{if } s = s', \\ \sigma^2 - \gamma(h) & \text{if } s \text{ and } s' \text{ are } h\text{-distant.} \end{cases} \tag{9}$$

By h-distant we mean that the two spatial locations s and s' have a spatial distance equivalent to h units. Hence, smaller h implies stronger dependence, and the case $s = s'$ is recovered by $h = 0$. In spatial statistics, it is common to assume that the second order properties of a process solely depend on the distance between locations, and not locations themselves. This

https://doi.org/10.5194/egusphere-2026-1016
Preprint. Discussion started: 19 March 2026

framework is referred to as spatial stationarity. This distance-based covariance will be made explicit in Section 4.2 (see (18)). If additional hierarchical levels or structured random effects (e.g., spatiotemporal random effects) are included, the covariance structure generalizes to account for more complex dependencies. For a more detailed discussion of random effects in GAMMs, including estimation and penalization techniques, we refer the reader to Wood (2017).

2.3 Estimation procedure

Let $\mathbf{A}_i$ and $\mathbf{P}_i$ denote the basis expansion model and penalty matrix for predictor f_i, $i \in \mathcal{I}$. To express (2) fully in linear terms, $\mathbf{W}_{s,t}$, $\mathbf{Z}_s$ and $\mathbf{A}_i$'s can be combined (column-wise) such that

$$\boldsymbol{\mathcal{X}}_s = \begin{pmatrix} \mathbf{W}_{s,t} & \mathbf{Z}_s & \mathbf{A}_1 & \cdots & \mathbf{A}_d \end{pmatrix} \tag{10}$$

becomes the global model matrix of model (2). Note that we assume that the cardinality of $\mathcal{I}$ is d in the sequel. Moreover, the global penalty term can be expressed as $\sum_{i'} \lambda_{i'} \boldsymbol{\theta}' \boldsymbol{\mathcal{P}}_{i'} \boldsymbol{\theta}$, where $\lambda_{i'}$ are positive smoothing parameters and $\boldsymbol{\theta}$ is a concatenation of coefficients $\boldsymbol{\beta}$, $\mathbf{u}$ and $\boldsymbol{\alpha}_i$'s. Here, we use $i' \neq i$ to denote the number of terms that are penalised. The matrix $\boldsymbol{\mathcal{P}}_{i'}$ is a block diagonal matrix such that $\boldsymbol{\theta}' \boldsymbol{\mathcal{P}}_{i'} \boldsymbol{\theta} = \boldsymbol{\alpha}_i' \mathbf{P}_i \boldsymbol{\alpha}_i$. Additionally, blocks should be such that unpenalised terms lead to a null summand in the sum. Indeed, i' differs from i as coefficients associated with $\boldsymbol{\beta}$ do not require penalisation.
Therefore, the GAMM can be expressed as the over-parametrised GLM

$$g(\mu_s(\mathbf{X}_{s,t})) = \boldsymbol{\mathcal{X}}_s \boldsymbol{\theta}, \quad Y_s(t) \sim \text{EF}(\mu_s(\mathbf{X}_{s,t}), \phi), \tag{11}$$

where the optimisation problem

$$\boldsymbol{\theta}^* = \arg\min_{\boldsymbol{\theta}} \left[D(\boldsymbol{\theta}) + \sum_{i=1}^{d} \lambda_i \boldsymbol{\theta}' \boldsymbol{\mathcal{P}}_i \boldsymbol{\theta} \right] \tag{12}$$

is our main focus. Here, $D(\boldsymbol{\theta})$ is the model deviance, defined as twice the saturated log-likelihood minus the log-likelihood. Usually, it is not possible to write (12) as a tractable expression. To remedy this issue, Wood (2010) introduces an iterative procedure to find optimal $\boldsymbol{\theta}$ and $\boldsymbol{\lambda}$ using a Laplace approximate marginal likelihood estimation. For the sake of readability, we do not summarise the estimation algorithm but simply refer to Wood (2010).

2.4 Regression diagnostics

In addition to the standard regression diagnostic tools for GAMs, we employ the `DHARMa` package introduced by Hartig (2024) to assess the adequacy of the fitted GAMM. For more traditional approaches see Wood (2017) and the `mgcv` package Wood and Wood (2015) in the R programming language. `DHARMa` provides diagnostics for hierarchical regression models (DHARMa), building upon the residual simulation framework described in Dunn and Smyth (1996); Gelman and Hill (2007). Traditional residuals in models with non-Gaussian responses can be difficult to interpret due to their dependence on the mean-variance relationship and non-linear link functions. DHARMa overcomes these limitations by generating standardized residuals through a simulation-based approach, ensuring uniformity under the correct model specification. The main idea behind DHARMa is the

https://doi.org/10.5194/egusphere-2026-1016
Preprint. Discussion started: 19 March 2026

following. Given the fitted GAMM, DHARMa generates multiple simulated datasets by drawing new response values from the conditional distribution of the fitted model. Then, the observed response values are ranked relative to the simulated distributions at each data point. The residuals are then computed as empirical cumulative distribution function values, ensuring they follow a uniform distribution, in the absence of model misspecification. This transformation makes it easier to identify systematic deviations from model assumptions, such as misspecified variance structures, zero inflation, or residual autocorrelation. A variety of statistical tests are provided in `DHARMa`, offering a more robust evaluation of model performance, particularly when working with complex data structures and mixed models.

3 Data and Study Area

Traditional paleoflood hydrology reconstructs the frequency and magnitude of past floods using geological evidence, such as flood deposits or geomorphological features in the river system (see Kochel and Baker (1982)). Over the past 30 years, paleoflood markers have raised further attention in modelling individual extreme floods. Another technique to obtain a complete flood series is to use lake sediment cores. There, abundant flood layers can be dated according to their position in the sediment core. The temporal resolution depends on the dating techniques. In annually laminated lake sediments, each year can be assigned to a particular layer providing a precise time (e.g. Swierczynski et al. (2013)). The most comprehensive dataset of long-term, continuous geology-based flood records from the European Alpine region was recently analysed in Wilhelm et al. (2022) . They studied how temperature changes affect flood hazards for different periods of history. Inspired by the latter work and by Albrecher et al. (2019), we aim to use these flood records to infer a spatial and temporal model for the number of floods in a given time period, focusing on the empirical dependence structure of flood risk over time and space. Given the yearly temporal resolution of the data, it would be possible to study a GAMM which focuses on yearly flood probabilities. However, for reasons that are showcased later, we have decided against this approach.

The dataset from Wilhelm et al. (2022) collects paleoflood data of $n = 27$ lakes in the European Alps (see Figure 1 for their locations). That is, the dataset contains the number of floods that occurred in each year. The available time span of the record varies across different lakes and ranges from the last 150 to the last 9,050 years (starting from 2000 CE; note that the common era (CE) time scale is generally used in flood risk analysis). Additionally, the dataset includes detailed information on each lake's location and physical characteristics. Specifically, we know geographic characteristics such as longitude and latitude (expressed in decimal degrees (DD)), altitude (expressed in meters above sea level), size of its catchment area (in squared kilometres) and the maximal elevation point of that area (also in meters above sea level). Furthermore, in Wilhelm et al. (2022, Extended Data Table 1) we find a variable that provides information about the timing of floods during a given year. This variable, named "flood season", indicates whether floods are more likely to happen in spring, summer, autumn, winter or any combination of these. For example, some lakes are reported to have spring and/or summer as their flood season. Lakes for which the flood season is unknown have been grouped together.

https://doi.org/10.5194/egusphere-2026-1016
Preprint. Discussion started: 19 March 2026

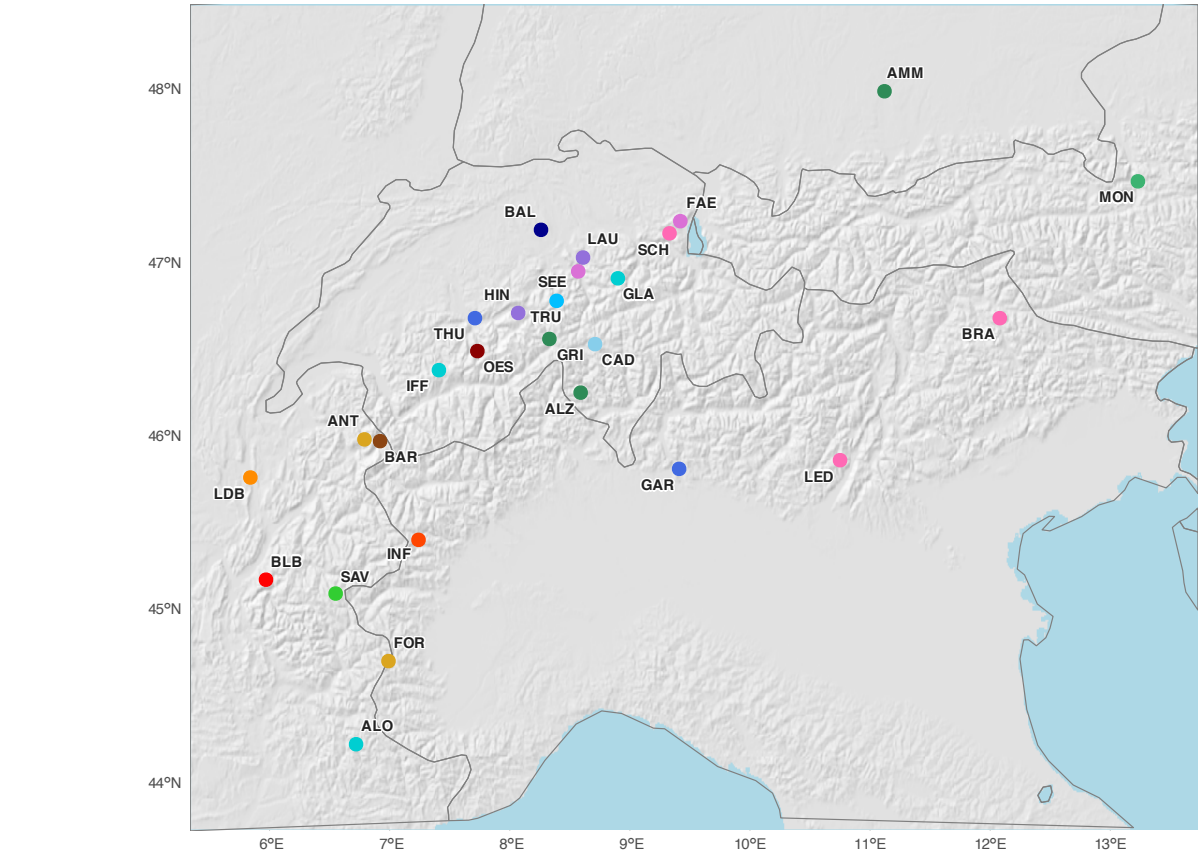

Figure 1. Locations of alpine lakes associated with sediment records. Unique colors identify individual lakes. The plot was created in `R` with packages `geodata` (Hijmans, 2025), `terra` (Hijmans et al., 2026), and `rnaturalearth` (Massicotte and South, 2026).

The dataset for our study exhibits varying availability of flood data across different lakes, with complete records spanning 9,050 years for only eight lakes (cf. Figure 2). Due to this inconsistency and the potential numerical instability of estimating regression predictors over the entire period with such a small sample, we consider a single GAMM that employs the longest time resolution for which most information is available, namely the last 1,450 years.

4 Spatio-temporal Model Specification

In this section, we implement the techniques described above to develop a spatial and temporal model that studies flood risk in the European Alpine region.

https://doi.org/10.5194/egusphere-2026-1016
Preprint. Discussion started: 19 March 2026

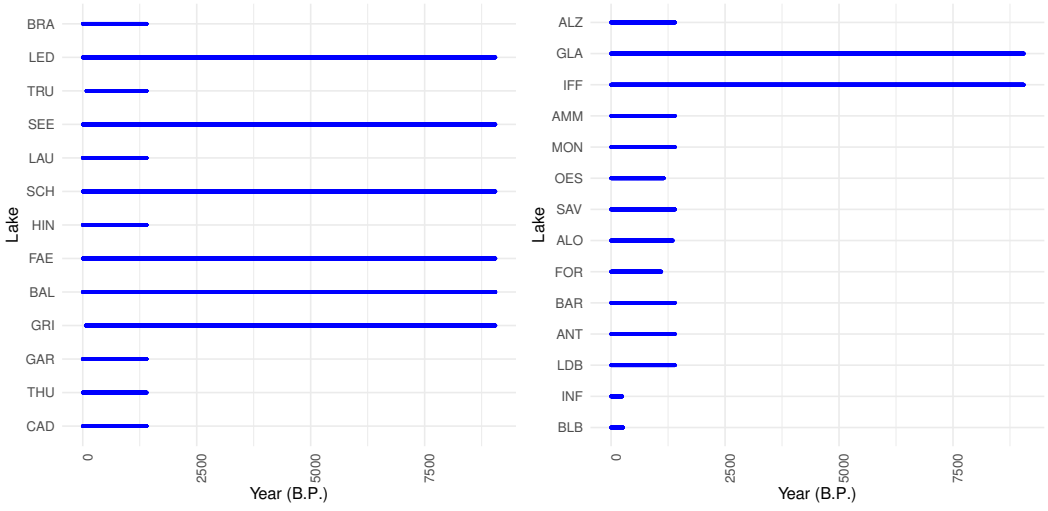

Figure 2. Temporal resolution of sediments records in Wilhelm et al. (2022). For each lake, we observe how far back into the past a sediment record spans. Blue-coloured dots correspond to years with observed values. Only seven records are complete, while others reach approximately 450 CE. Also, three of them have missing values in more recent years. The time scale employed is time Before Present (B.P.), where 1,950 CE is chosen as the reference point.

4.1 Increment of a counting process

As discussed previously, it would have been possible to model yearly flood probabilities directly using a GAMM. We explored this approach, but found that no specification could avoid assumption violations: residuals from candidate models exhibited strong patterns and systematic dependence on covariates, and overall predictive performance, for instance measured by deviance explained, was unsatisfactory.

Motivated by the theory of doubly stochastic Poisson processes driven by Lévy subordinators (Selch et al., 2018), we therefore focus instead on increments of the flood counting process. Specifically, let $N_s(t)$ denote the number of floods at time t and location s, and define the increment over a time interval $(t, t+\tau]$ as

$$Y_s(t,\tau) := N_s(t+\tau) - N_s(t). \tag{13}$$

The increment $Y_s(t,\tau)$ is assumed to follow a Negative Binomial distribution, with conditional expectation given by the GAMM specification in (2) and variance

$$\mathrm{Var}(Y_s(t,\tau)) = g^{-1}\left(\eta_s(t,\tau)\right)\left(1 + \frac{g^{-1}\left(\eta_s(t,\tau)\right)}{\gamma}\right), \tag{14}$$

where γ is a dispersion parameter, and the expectation also depends on the length of the increment τ. Alternatively, the increments can be represented in a Cox process framework as

$$Y_s(t,\tau) \sim \mathrm{Poisson}(M_s(t,\tau)), \tag{15}$$

https://doi.org/10.5194/egusphere-2026-1016
Preprint. Discussion started: 19 March 2026

with $M_s(t,\tau)$ following a Gamma distribution,

$$M_s(t,\tau) \sim \Gamma\left(\gamma, \frac{\gamma}{g^{-1}(\eta_s(t,\tau))}\right). \tag{16}$$

It is important to note that, due to the GAMM formulation, our model does not fully recover a doubly stochastic Poisson process with a Gamma (Lévy) subordinator. Incorporating the starting time t into the moments of the distribution leads to non-stationary increments, and the shape parameter of the Gamma distribution is independent of the increment length τ. While it would be possible to parametrise the model such that increments correspond to those from a stationary Cox process (Albrecher et al., 2017, Ch.5.2.4), we do not pursue this approach here. In practice, assuming stationary increments is too restrictive for natural processes like floods, where time itself influences the distribution estimated by (2). Nonetheless, the connection to stationary Cox processes provides a useful conceptual link and offers a natural interpretation of the model in terms of increments of a counting process.

4.2 Spatio-temporal model

In the subsequent analysis, we describe the GAMM model used to study the increments (13).
The conditional expectation is assumed to originate from

$$\begin{aligned}\eta_s(t,\tau) = \log\left(\mu_s(\mathbf{X}_{s,t.\tau})\right) = &\log(\tau) + \beta + u_s + b_{\text{season}}(s) + \\ &f_{\text{time}}(t) + f_{\text{space}}(s) + f_{\text{space-time}}(s,t) + \\ &f_{\text{alt}}(\text{alt}_s) + f_{\text{ca}}(\text{ca}_s) + f_{\text{caalt}}(\text{caalt}_s).\end{aligned} \tag{17}$$

The time interval of the increment is used as an offset, such that the remaining terms of $\exp(\eta_s(t,\tau))$ can be understood as the probability to have a “flood year". Indeed, the conditional expectation becomes the product of the number of years considered and the remaining exponential term, which can be regarded as a probability whenever $\eta_s(t,\tau) \leq 0$. Moreover, using τ as an offset separates the effect of predictors from the size of the time interval considered. The coefficient β is a simple regression coefficient, which is complemented by $f_{\text{time}}(t)$ to model a baseline conditional expectation across time. Deviations from the shared mean function are explained by the remaining feature-dependent predictors.

We introduce two separate random effects vectors $\mathbf{u} \sim N(0, \mathbf{\Sigma}_s)$ and $\mathbf{b} \sim N(0, \mathbf{\Sigma}_{\text{season}})$ to introduce correlation between increment realisations observed at the same location s and, through $\mathbf{\Sigma}_s$, between nearby locations, as well as for lakes that have the same flood season. Here, $\mathbf{\Sigma}$ denotes a general covariance matrix which we compute empirically. These random effects can be interpreted as adjusting coefficients that lead to a more precise estimation of conditional means, while accounting for correlation within and between nearby locations. They can also be considered as variables that capture the effect of non-measured features that might play a role in describing the distribution of data. In our particular case, we do not have many sampling locations or many covariates to determine the distribution under study. Therefore, the use of random effects is justified.

Regarding $\mathbf{u}$, a distance-based dependence notion is considered for $\mathbf{\Sigma}_s$, such that lakes close to each other have stronger correlation than lakes that are further away. We briefly describe how to introduce this type of dependence in random intercepts.

https://doi.org/10.5194/egusphere-2026-1016
Preprint. Discussion started: 19 March 2026

We adopt the methodology given in Pebesma (2004). First, a distance matrix $d_{ij} = \|\mathbf{s}_i - \mathbf{s}_j\|_2$ is obtained, where $d_{ij} = d_{ji}$, $d_{ii} = 0$ and $i, j = 1, \ldots, 27$. Then, the omnidirectional empirical semivariogram

$$\hat{\gamma}(h) = \tfrac{1}{2} \operatorname{Var}\left(Y_{s_i}(t,\tau) - Y_{s_j}(t,\tau) \,\middle|\, d_{ij} \approx h\right) \tag{18}$$

is computed. The empirical semivariogram (18) is then used to fit the following parametric model

$$\gamma(h) = c_0 + c_1 \left(1 - e^{-h/\rho}\right), \tag{19}$$

by solving the optimisation problem $(c_0^*, c_1^*, \rho^*) = \arg\min_{c_0, c_1, \rho} \sum_h \left(\gamma(h) - \hat{\gamma}(h)\right)^2$ for some distances h. The fitted parameters are then translated into the covariance function

$$\{\boldsymbol{\Sigma}_s\}_{ij} = c_0^* + c_1^* \, e^{-d_{ij}/\rho^*}, \qquad i, j = 1, \ldots, 27, \tag{20}$$

which emulates an isotropic Gaussian random field, namely a continuous spatial Gaussian process whose covariance only depends on the magnitude of the distances between locations, with exponential correlation. Finally, the resulting matrix $\boldsymbol{\Sigma}_s$ is inverted to give the penalty matrix $\mathbf{P} = \boldsymbol{\Sigma}_s^{-1}$ used for the spatial random intercepts in (17). Note that there exist many alternatives to the exponential model (19), but this discussion is outside the scope of our analysis. We instead refer the interested reader to Cressie (1993); Hristopulos (2020) for more details on the subject.

Besides longitude and latitude, catchment characteristics are assumed to have a non-linear effect on the additive score. These (possibly) non-linear functions aim at reflecting the complexity of weather patterns in alpine areas. They acknowledge the multi-faceted nature of flood occurrences, which are influenced by factors such as altitude, precipitation, soil moisture, and snowmelt.

A two-dimensional smooth function captures the effect of locations s (longitude and latitude) on flood occurrences, while a three-dimensional predictor captures the interaction between location s and time t. The function f_{space} aims at explaining the variability over the bounded spatial extent of the Alps considered (see Figure 1). A smoother soap film (see Wood et al. (2008)) is used for the spatial marginal basis in f_{space} to avoid artificial boundary effects. We use the same marginal bases for the interaction term $f_{\text{space-time}}$, and thin-plate splines are used as temporal basis functions. We let spatial predictors vary non-linearly, as the European Alpine region is affected by different climatic effects over time and space. For example, small catchment areas are affected by local short-duration convective storms with high intensities more than long-duration synoptic storms (see Blöschl et al. (2019)). Note that we employ (7) as penalty terms, to identify if smooth functions in (17) are necessary.

In principle, the model in (17) could be more complex. It would be possible to incorporate more interaction terms or to assume a varying coefficient model where all predictors are free to vary across the spatial region or temporally. Given the small number of observations at our disposal, a more complex additive score does not necessarily lead to a better performance. Moreover, a complex model is more likely to suffer from over-fitting. Increasing the number of basis functions used in expansion (3) can also increase model complexity. One of the drawbacks of GAMs is that the number of basis functions needs to be pre-specified. One needs enough basis functions to not under-smooth the data, and at the same time, only a few to not run into over-fitting problems. In the following application, we keep the `mgcv` default number of basis functions.

https://doi.org/10.5194/egusphere-2026-1016
Preprint. Discussion started: 19 March 2026

5 Results

5.1 Flood risk during the last 1,450 years

Our application focuses on the time period for which the most observations are available, spanning 1,450 years from 550 CE to 2,000 CE. We model increments of length $\tau = 20$ years, so that the response variable in the GAMM represents the number of floods occurring within each 20-year interval. This choice of τ balances the need for sufficient data within each increment while ensuring that the model assumptions are respected and that residual patterns remain consistent with the theoretical specification.

The estimation results of (17) are summarised in Table 1. Significant predictors identified by the GAMM include the fixed effects $\widehat{\beta}$, random intercepts $\widehat{u}_s$, and smooth functions representing temporal, spatial, and space-time interactions ($\widehat{f}_{\text{time}}$, $\widehat{f}_{\text{space}}$, $\widehat{f}_{\text{space-time}}$). In contrast, smooth terms corresponding to flood seasonality, altitude, and catchment characteristics are penalised to zero, indicating that these factors do not contribute additional explanatory power once the other smooth terms are included. Model fit metrics further confirm satisfactory performance: the coefficient of determination is $R^2 = 0.624$, and the proportion of deviance residuals explained is 0.551, showing that the model captures a substantial fraction of the variability in the observed increments over the last 1,450 years.

Parametric terms	Estimate	Std. Error	z value	Pr(>|z|)
$\widehat{\beta}$	-2.418	0.257	-9.412	0.000
Smooth terms	**edf**	**Ref.df**	**Chi.sq**	**p-value**
$\widehat{u}_s$	18.355	26	193.433	0.000
$\widehat{b}_{\text{season}}(s)$	2.731	8	26.600	0.201
$\widehat{f}_{\text{time}}(t)$	9.920	29	32.422	0.000
$\widehat{f}_{\text{space}}(s)$	4.146	26	3160.734	0.005
$\widehat{f}_{\text{space-time}}(s,t)$	26.170	100	115.402	0.000
$\widehat{f}_{\text{ca}}(\text{ca}_s)$	0.000	19	0.000	0.869
$\widehat{f}_{\text{caalt}}(\text{caalt}_s)$	0.000	19	0.000	0.999
$\widehat{f}_{\text{alt}}(\text{alt}_s)$	0.002	19	0.001	0.494
Model fit		-REML	R^2	Deviance exp.
		-2639.400	0.624	0.551

Table 1. Summary statistics for the GAMM terms.

Note that the overall expectation for all locations in the Alps is $\tau \exp\left(\widehat{\beta}\right) = 1.782$ floods per 20-year period, which serves as the baseline estimate. The effect of any estimated predictor on this baseline is expressed through the multiplicative term $\exp\left(\widehat{f}(\cdot)\right)$, capturing deviations from the overall expectation in a flexible, interpretable manner.

Random intercept estimates are shown in Figure 3 and represent lake-specific deviations from the baseline $\tau \exp\left(\widehat{\beta}\right)$, acting as shifts on the common functional intercept. Positive values of $\widehat{u}_s$ indicate that a lake is more likely to experience floods than the overall average, while negative values indicate a lower likelihood. For most lakes, the 90% confidence intervals of these

https://doi.org/10.5194/egusphere-2026-1016
Preprint. Discussion started: 19 March 2026

estimates are wide, yet several lakes exhibit significant deviations. Notable examples include Mondesee, du Bourget, Glattalp, Anterne, and Allos in the left panel, and Trueb, Thun, Garlate, Faelen, Cadagno, and Baldegg in the right panel. In particular, Lakes Inferiore di Laures, Ledro, and Oeschinen show approximately double the baseline probability of flood events, whereas Lakes Iffig, Saviese, and Grimsel display roughly half the baseline probability.

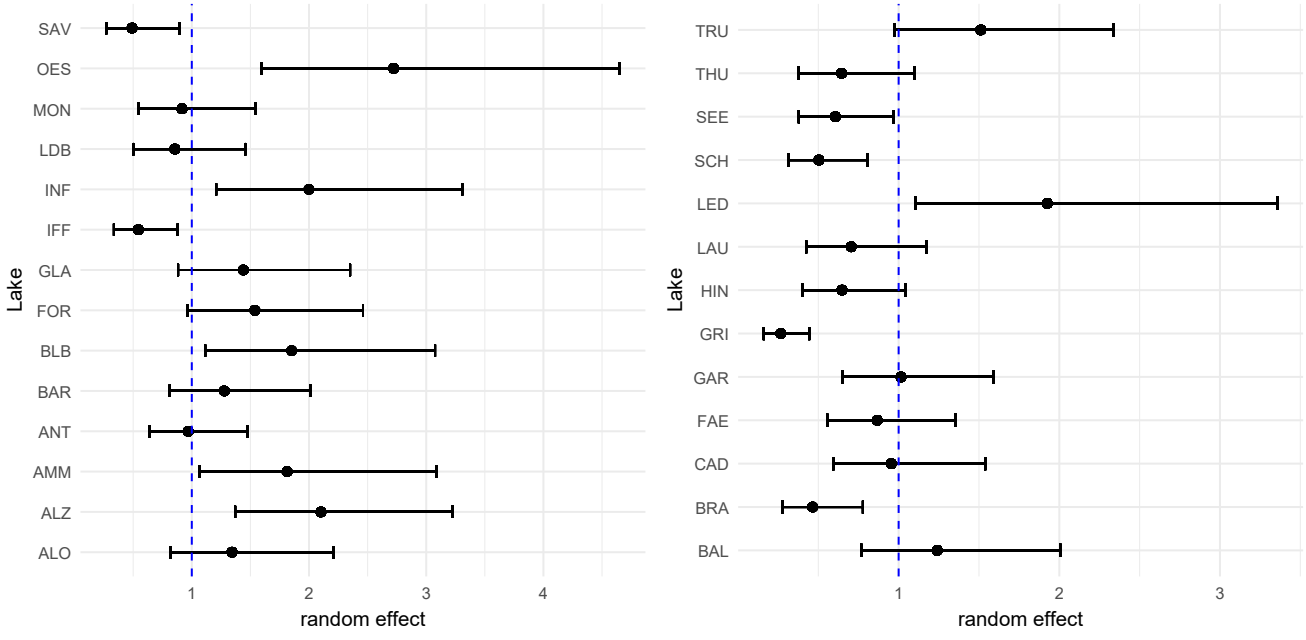

Figure 3. Error bar plot of estimated random intercepts $\exp(\widehat{u}_s)$ for each lake, along with its 90% point-wise confidence interval.

We proceed by examining the smooth functional terms identified as significant (note that the season effect $\widehat{b}_{\text{season}}(s)$, as well as $\widehat{f}_{\text{alt}}$, $\widehat{f}_{\text{ca}}$, and $\widehat{f}_{\text{caalt}}$, are not significant).

Figure 4 displays the estimated functional predictor $\exp\left(\widehat{f}_{\text{time}}(t)\right)$ with its point-wise 90% confidence interval, revealing the non-stationary nature of flood occurrences over time. Rather than following a uniform monotone trend, the time effect exhibits periods of increasing and decreasing flood activity. For example, flood risk is about 20% lower in 555 CE, gradually intensifies until around 710 CE, and then declines again. The lowest values occur prior to the Oort Solar Minimum (1010–1140 CE). After 876 CE, a sharp rise is observed, peaking around 1340 CE, followed by a gradual decrease until 1670 CE. A modest increase occurs between 1670 and 1840 CE, after which the time effect slightly declines, before trending upward again in the most recent years. This temporal pattern highlights the complex, non-linear evolution of flood occurrences across the last 1,450 years.

Overall, we observe a clear increase in the expected number of floods over 20-year periods since 550 CE. This aggregate pattern is consistent with the findings of Schmocker-Fackel and Naef (2010), who reported that flood activity in Swiss catchments alternated between periods of higher and lower frequency, independent of catchment size. They also noted a recent increase in

https://doi.org/10.5194/egusphere-2026-1016
Preprint. Discussion started: 19 March 2026

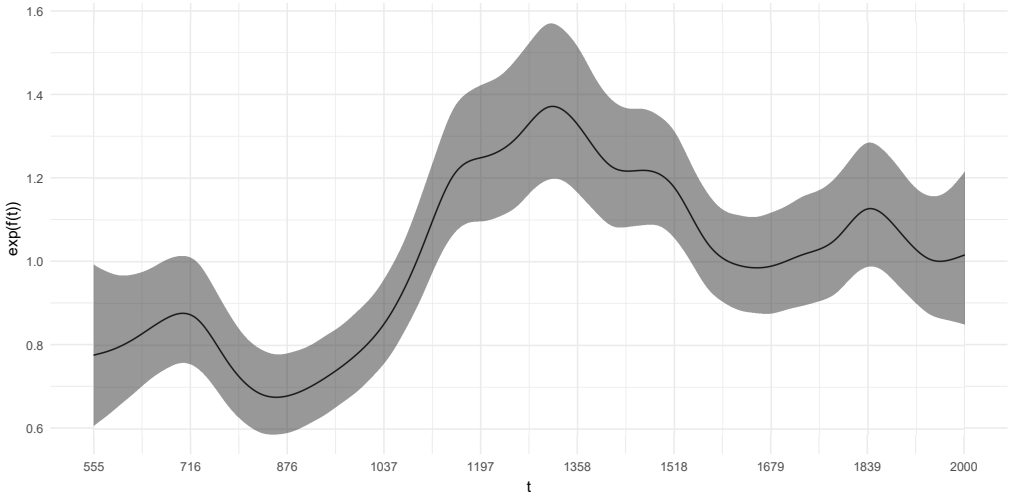

Figure 4. Smooth functional intercept $\exp\left(\widehat{f}_{\text{time}}(t)\right)$, describing the effect of time on the additive score. The grey ribbon depicts the 90% point-wise confidence interval.

flood activity starting in the 1970s, which is only partially captured in Figure 4. Similarly, Ruiz-Villanueva and Molnar (2020, Sec. 3.3) found that European flood frequencies over the last 500 years exhibit variations on timescales of 30 to 100 years. The fluctuations observed in Figure 4 suggest that flood frequencies are influenced by long-term climatic and environmental factors that are not directly observed in our model. This aligns with previous studies indicating alternating flood-rich and flood-poor periods, reinforcing the view that historical flood occurrences follow cyclic, non-stationary patterns rather than a constant trend. For comparison and as a consistency check, Figure 5 shows the total number of floods across all lakes aggregated in 20-year windows, together with a moving average with a bandwidth of 20 years. As expected, this aggregation smoothes out short-term variations, resulting in less pronounced fluctuations than those depicted in Figure 4. The two figures would only coincide closely if the lake sites were relatively uniformly distributed across space.

Figure 6 shows the estimated spatial predictor $\exp\left(\widehat{f}_{\text{space}}(s)\right)$, highlighting clear regional differences in flood risk across the European Alps. This surface represents the broad-scale spatial trend after accounting for lake-specific random intercepts; the distribution of $\widehat{u}_s$ (with covariance $\boldsymbol{\Sigma}_s$) captures additional location-level deviations not explained by the smooth spatial term. Averaged over time, the central Alpine region (blue-colored area) is less prone to floods, whereas the South-Western region exhibits the highest values, with a factor of 1.2 corresponding approximately to a 20% increase in flood risk conditional on all other predictors. Extending this analysis in both space and time, Figure 7 presents the space-time predictor $\widehat{f}_{\text{space-time}}(s,t)$, which captures how regional flood risk evolves over the last 1,450 years. The soap smoother used in the estimation assigns null values to coordinates at the Alpine boundaries, preventing boundary artifacts and ensuring smooth estimates across the domain. At the beginning of the period ($t = 550$ CE), most of the Alps show relatively low flood risk, except for elevated risk in the South-Western-most and North-Eastern-most areas. By $t = 734$ CE, the Eastern Alps display heightened risk, which reverses around $t = 1420$ CE with increased flood probability in the Western region, a pattern consistent with historical observations of

https://doi.org/10.5194/egusphere-2026-1016
Preprint. Discussion started: 19 March 2026

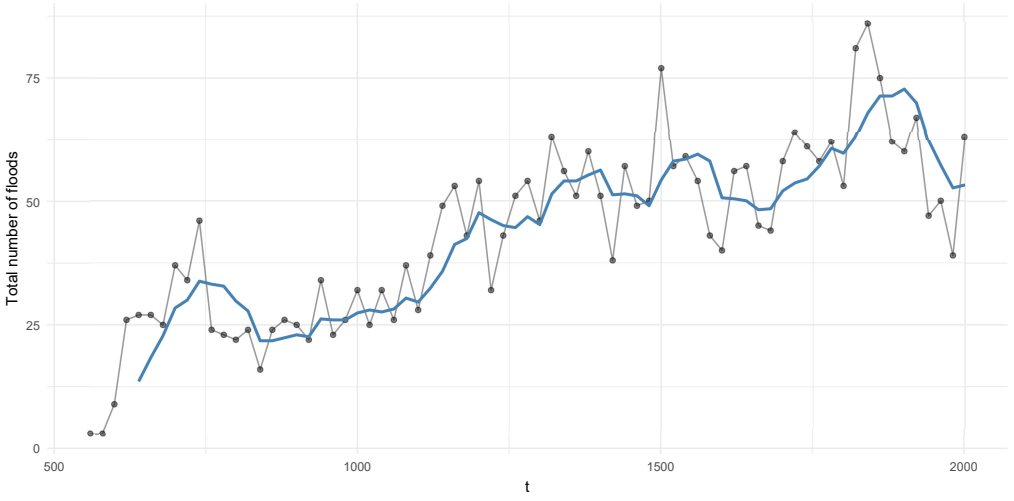

Figure 5. Moving average (bandwidth 20 years) of total number of floods across the 27 lakes (blue) versus actual batch counts across consecutive 20 year periods (grey).

reduced flood activity in Central-Eastern Europe (Brázdil et al., 2005; Mudelsee et al., 2003). Differences are less pronounced by $t = 1645$ CE, but the following two centuries show amplified regional variability, with increased flood frequency in the central Alps. In the most recent period ($t = 2000$ CE), the central region exhibits relatively lower flood risk compared to surrounding areas, aligning with instrumental records (Blöschl et al., 2015). Collectively, these spatio-temporal variations reveal distinct hydroclimatic sectors within the European Alps and illustrate the strong sensitivity of regional flood patterns to both natural variability and climate change (Blöschl et al., 2019).

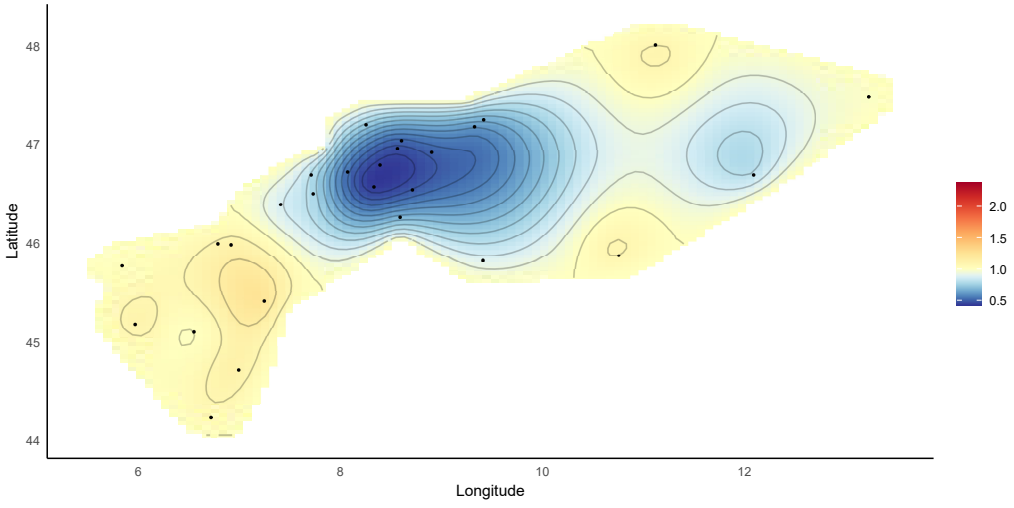

Figure 6. Estimated spatial predictor $\exp\left(\widehat{f}_{\text{space}}(s)\right)$. Black dots indicate the lakes' locations.

https://doi.org/10.5194/egusphere-2026-1016
Preprint. Discussion started: 19 March 2026

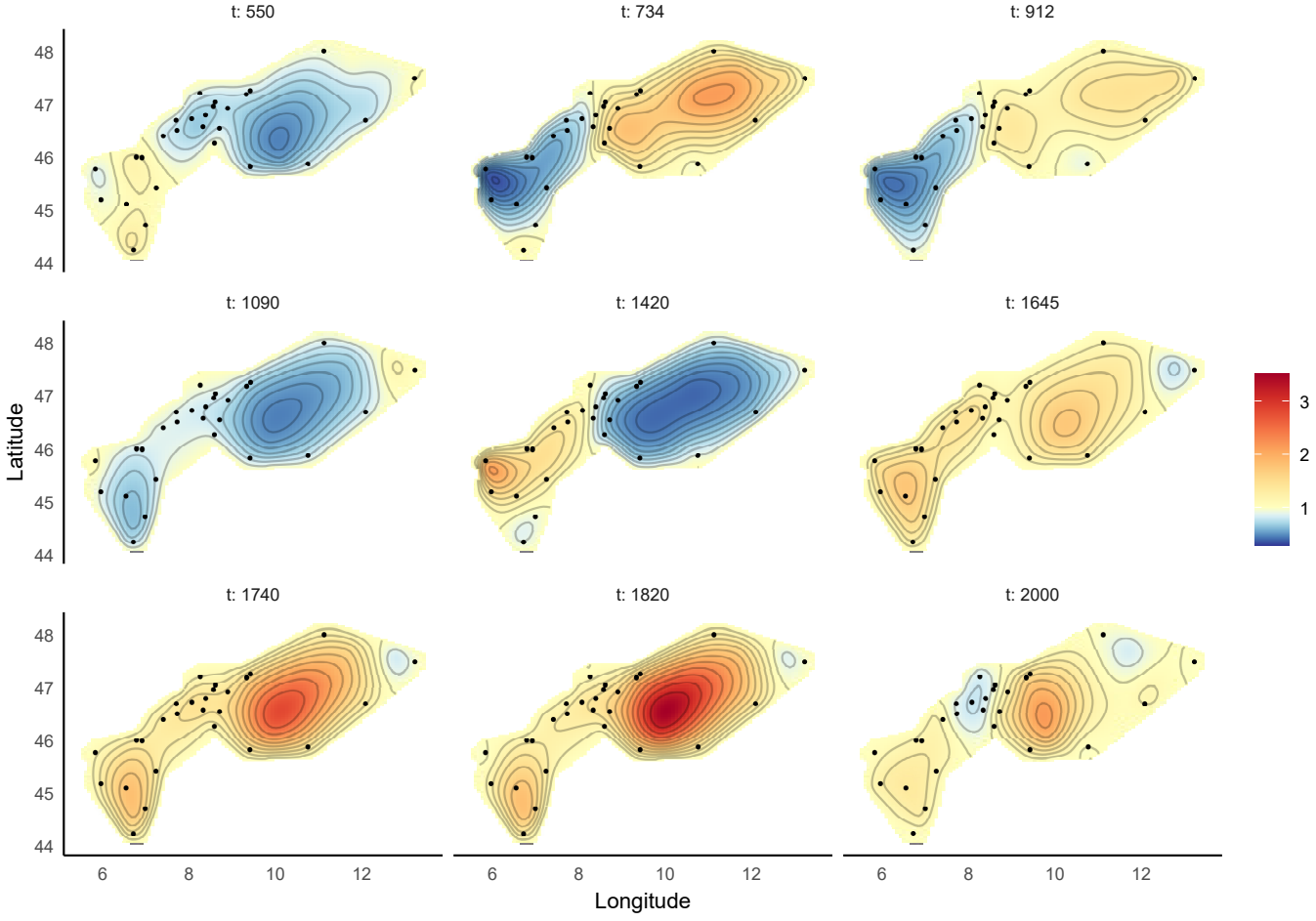

Figure 7. Estimated spatial predictor $\exp\left(\widehat{f}_{\text{space-time}}(s,t)\right)$ for selected time points. All the plots use the same colour grading. Black dots indicate the lakes' locations.

5.2 Model diagnostics

We now assess model adequacy through a detailed analysis of residuals. As discussed in Section 2.4, we follow the simulation-based diagnostic approach proposed by Hartig (2024), where residuals generated under a correctly specified model are expected to follow a uniform distribution. Figure 8 summarises the main diagnostic checks, displaying a QQ-plot of simulated residuals in the left panel and a residual-versus-fitted plot in the right panel. The QQ-plot shows close agreement between observed and expected uniform quantiles, with points following the main diagonal. This visual assessment is supported by a two-sided Kolmogorov–Smirnov test (Schröer and Trenkler, 1995), reported in the top left of the panel, which does not reject the null hypothesis of uniformity. In addition, simulation-based dispersion and outlier tests are performed, with both resulting p-values being non-significant, further indicating no major departures from the assumed model structure.

https://doi.org/10.5194/egusphere-2026-1016
Preprint. Discussion started: 19 March 2026

The residual-versus-fitted plot in the right panel of Figure 8 shows no systematic patterns, as would be expected under a well-specified model. The residuals form an approximately random cloud, and quantile regression curves fitted to the 25%, 50%, and 75% residual quantiles closely track the expected quantile locations of a uniform distribution (in particular the median at 0.5). While minor deviations are present, they remain small and do not suggest model misspecification. Further details on the interpretation of these diagnostic tests can be found in Hartig (2024) and the vignette accompanying the `DHARMa` package.

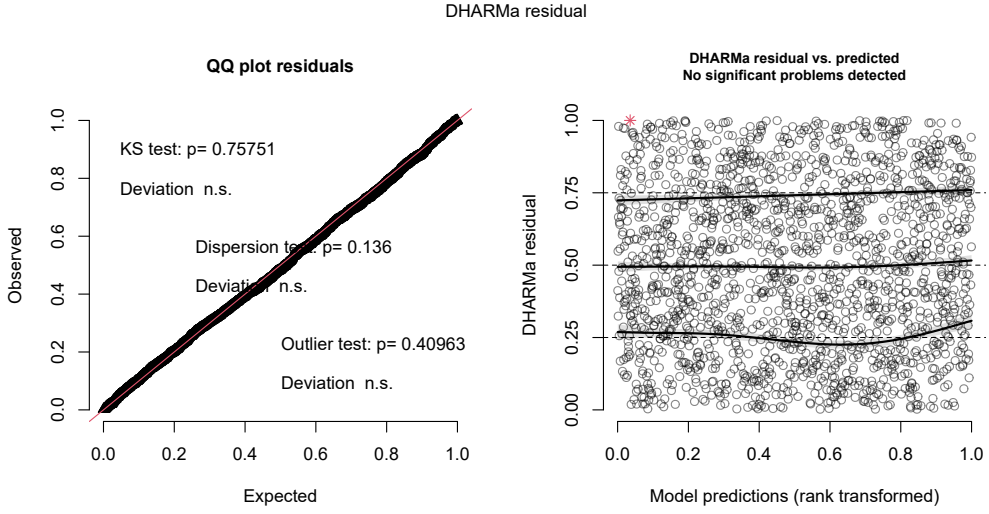

Figure 8. Standard diagnostic plots for simulated residuals in `DHARMa`. The left panel is a uniform QQ plot, and the right panel shows residuals against predicted values with outliers highlighted in red. P-values of KS, dispersion and outlier statistical tests are produced in the left panel. A quantile regression is performed on the residuals in the right panel for the 25%,50% and 75% quantiles.

Beyond global diagnostics, we also investigate whether residual structure remains with respect to individual covariates included in (17). Figure 9 presents box plots of residuals grouped by lake, together with tests for within-group uniformity and between-group homogeneity of variances. None of the lakes yields significant p-values in either test, although some locations, such as Lake Allos, exhibit slightly increased residual variability and come close to being flagged. A similar analysis grouped by flood seasonality is shown in Figure 10, where the Levene test indicates homogeneous variances across groups. Finally, residuals plotted against the remaining covariates (time, longitude, latitude, altitude, catchment area, and maximum catchment altitude) are displayed in Figure 11. No systematic patterns are apparent, aside from the discretisation effects induced by the limited number of spatial locations (27 values) and catchment characteristics available. In summary, these diagnostics suggest that the estimated model provides an adequate description of the data, particularly in view of the relatively small sample size.

https://doi.org/10.5194/egusphere-2026-1016
Preprint. Discussion started: 19 March 2026

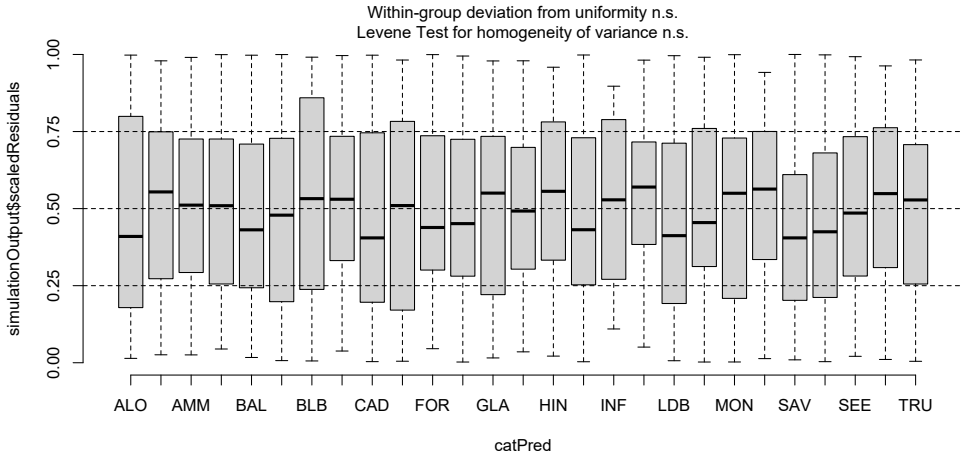

Figure 9. Box plots of model residuals grouped by Lake location. The top of the figure shows if the distribution assumption is violated for any lake (no issues in our case).

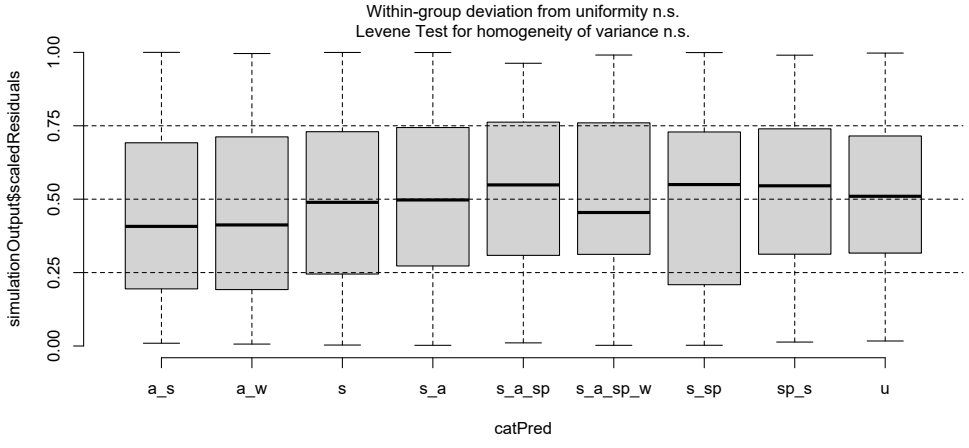

Figure 10. Box plots of model residuals grouped by flood season. The Levene test for variance homogeneity leads to the rejection of the null hypothesis.

6 Discussion and Conclusion

The use of GAMMs in this study provides a flexible framework to analyse flood occurrences by incorporating non-linear temporal and spatial dependencies, allowing us to account for long-term flood variations while accommodating regional heterogeneity. A key advantage of this approach lies in its ability to interpolate missing data and to capture non-stationary flood

https://doi.org/10.5194/egusphere-2026-1016
Preprint. Discussion started: 19 March 2026

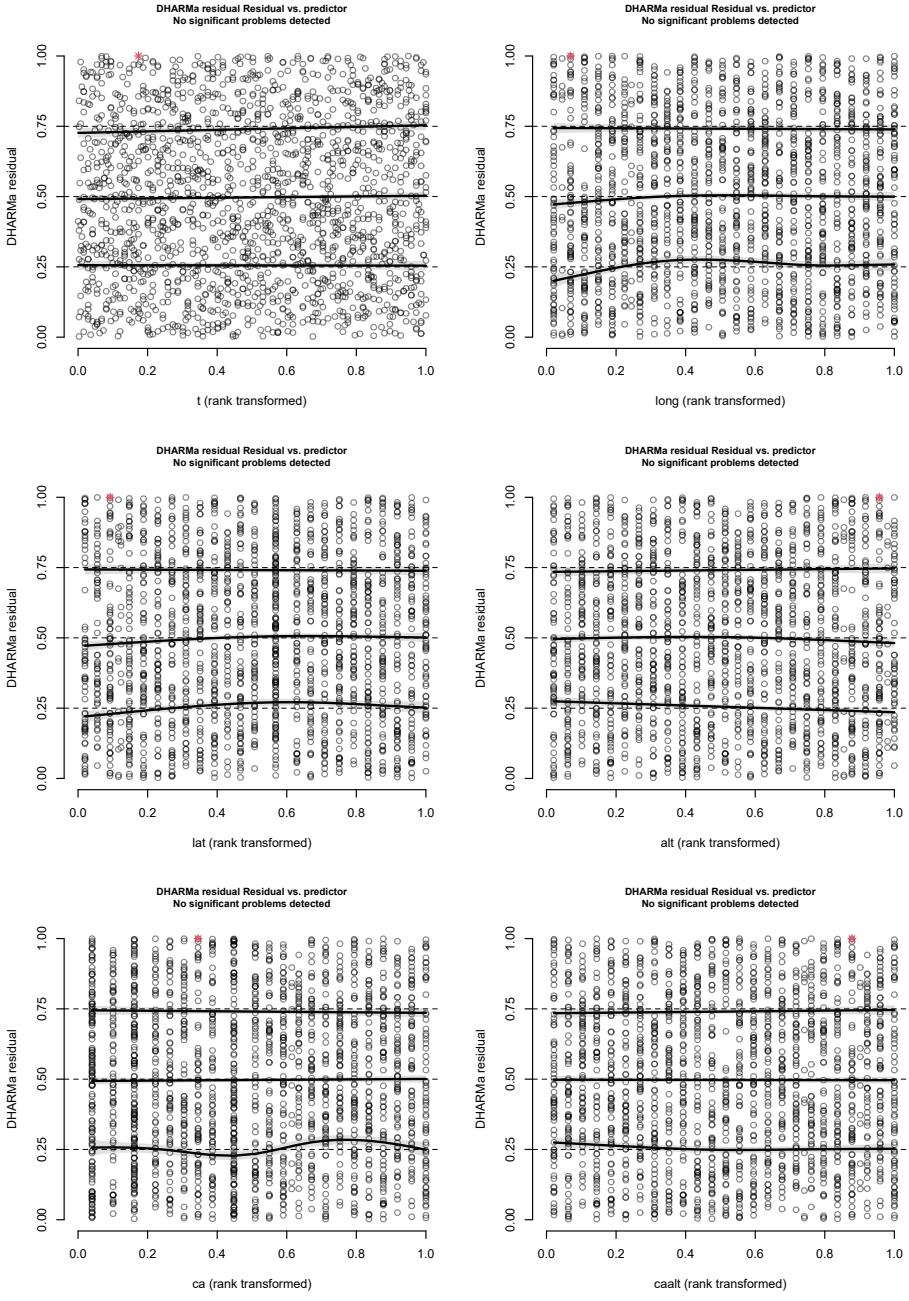

Figure 11. Residual plots for *t*, longitude (long), latitude (lat), altitude (alt), catchment area (ca) and maximum altitude of the catchment (caalt).

https://doi.org/10.5194/egusphere-2026-1016
Preprint. Discussion started: 19 March 2026

behaviour, which is essential for understanding historical flood patterns and their potential climatic drivers. The hierarchical structure of GAMMs further enables a principled representation of uncertainty associated with sediment-based flood records. The validation results presented in the previous section, together with the simulation analysis provided in the Appendix, are reassuring and indicate that the model captures many important features of the underlying flood dynamics. This is particularly noteworthy given that the analysis relies primarily on the sediment records and spatial coordinates of the 27 lakes, supplemented by features of their catchment areas. Interestingly, the latter did not provide additional predictive power, as the statistical procedure identified them as not contributing significant additional information to the explanation of joint flood occurrence. This suggests that much of the relevant signal is already contained in the spatio-temporal structure of the flood records themselves. One of the main purposes of this paper is therefore to illustrate the potential of additive methods for the analysis of flood risk over long historical periods and to advocate GAMMs as a useful and versatile tool for this research community. With increasing data resolution and availability, this approach is expected to become even more powerful and to help mitigate gaps and uncertainties that are inherent in long historical data series. In the present application, GAMMs were used to improve marginal flood occurrence estimates based on individual flood histories over the past 1,450 years by augmenting and stabilising them with information shared across locations.

A principal feature of the proposed methodology is the explicit incorporation of dependence structures in the modelling of flood occurrences, reflecting its inherently multivariate nature. Dependence is often overlooked in the existing literature, largely due to the additional complexity it introduces, and many previous studies rely on statistical methods that assume independence between flood records, either treating flood events as isolated occurrences or imposing stationarity on their temporal evolution. In contrast, the present approach allows for the inclusion of both fixed and random effects to capture correlations across time and space, acknowledging that flood occurrences are not independent but may exhibit clustering, periodicity, and regional variation driven by unobserved climatic and geomorphological factors. This dependence is introduced through several components of the model: smooth temporal trends capture non-stationary flood behaviour across different climatic periods, spatially structured random effects account for location-specific variation reflecting unobserved hydrological and topographical features, and the hierarchical structure of the model propagates dependencies between different lakes and catchment areas through the estimation process. Together, these components provide a more realistic representation of flood risk dynamics across time and space.

Despite these advantages, several limitations and scope restrictions of the present study must be acknowledged. The modelling framework depends on the availability of sediment records which, although extensive, are here confined to 27 lake sites in the Alps, implying a limited spatial resolution; a finer grid of observed locations would be expected to further sharpen the results. Moreover, while the model captures broad spatial patterns in flood occurrence, it does not explicitly incorporate hydrological processes such as catchment-specific runoff generation mechanisms, which could further enhance predictive performance. Potential extensions of the framework include the incorporation of additional covariates, both scalar and time-varying, provided that sufficiently long and spatially resolved data become available. One candidate is temperature, for which long records exist at selected locations based on speleothems and isotopic signatures (see, e.g., Waltgenbach et al. (2020)); however, such data were not available on a sufficiently fine spatial grid for inclusion here, and it remains unclear whether local

https://doi.org/10.5194/egusphere-2026-1016
Preprint. Discussion started: 19 March 2026

temperature alone constitutes a sufficiently strong driver of flood occurrence to improve the model beyond the information already contained in the flood records themselves. Other climate-related covariates, such as timberline reconstructions Tinner and Ammann (2001) or landslide records Borgatti and Soldati (2010), represent further promising directions, but their availability was likewise insufficient for inclusion in the present study. Finally, while the modelling approach enhances the understanding of both temporal and spatial dimensions of flood risk, the resulting flood occurrence curves cannot yet be directly used for the simulation of annual flood occurrences at the regional scale, as joint flood occurrence in neighbouring areas would need to be modelled explicitly (see Albrecher et al. (2020)). In addition, the curves cannot be directly assigned to locations between or beyond the 27 lakes considered, as this would implicitly assume that each such location represents a catchment sink. With appropriate adaptations incorporating detailed topographical information, the framework could nevertheless be extended towards a more continuous spatio-temporal risk assessment, potentially enabling refined risk maps with location-specific return periods at a much finer resolution than those currently in use.

In summary, the fitted GAMM suggests an overall increase in expected flood counts over the last 1,450 years, with pronounced regional differences captured by the spatial and space-time smooths, while catchment characteristics (altitude, catchment area, maximum catchment elevation) do not add explanatory power once spatio-temporal effects are included. Lake-specific deviations from the regional mean are absorbed by random intercepts that shift the baseline where supported by data. These findings highlight the value of additive modelling for long historical flood records, and suggest that denser spatial coverage and a clearer seasonal separation of flood types would further improve inference (Glur et al., 2013). Looking ahead, alternative approaches such as embedding flood likelihood curves in space using time-varying kriging (Giraldo et al., 2010; Mateu and Giraldo, 2021) could complement the present framework and help build finer-resolution risk maps. This ambition aligns with current paleoflood initiatives, including the Floods Working Group 2024–2026, which aims to integrate extreme-flood reconstructions into modern risk assessment workflows (PAGES – Past Global Changes, 2025).

Code and data availability. The lake sediment data used in this study is publicly available at https://www.ncei.noaa.gov/access/paleo-search/study/34712 (Wilhelm et al., 2022). The R code developed for the statistical analysis and modeling is available from the corresponding author upon request.

Appendix A: Simulation of counting processes

The GAMM considered in our application can be used to simulate sample paths of the stochastic counting processes underlying flood occurrences. Recall that, conditional on covariate information, the increments are independent. For a given location, we can therefore simulate one realization per time interval, and by summing these increments, we obtain a sample path of the originating counting process. Figures A1 to A3 show the results of such simulations for each Alpine lake included in our study. Each panel presents 1000 simulated sample paths, with the average path compared to the observed counting process. For almost

https://doi.org/10.5194/egusphere-2026-1016
Preprint. Discussion started: 19 March 2026

all lakes, the expected simulation closely follows the observed realizations, indicating that the model successfully captures the temporal dynamics of flood occurrences.

For lakes with restricted temporal resolution, the observed increments are aligned with the expected simulation path. That is, it is assumed that the unobserved increments prior to the first observation correspond to the expected simulation, allowing us to evaluate whether the trend of the counting process is correctly captured by the model, independently of the total number of floods that may have occurred before observations begin. For example, in Figure A1, Lakes Blanc de Belledone (BLB) and Inferiore di Laures (INF) have data only for the most recent 200 years. By initializing the observed increments from the expected simulation path, the predicted number of floods aligns well with the trend observed in the available data.

An additional benefit of these plots is that they provide a visual check on whether a homogeneous Poisson process would be a reasonable modeling choice. Such a process would correspond to a linear, steadily increasing sample path. However, in most cases, the observed curvature in the simulated paths indicates that more flexible models, such as Cox processes, are better suited to describe the observed count data.

Author contributions. HA, MLB, and MB conceptualized the methodological ideas, contributed to the writing, and edited the manuscript. AJAM performed the statistical analysis, led the writing of the original draft, and contributed to the editing. TS provided the dataset and contributed to the editing of the manuscript.

Competing interests. The contact author has declared that none of the authors has any competing interests.

Acknowledgements. MB acknowledges support from the Carlsberg Foundation, grant CF23-1096.

https://doi.org/10.5194/egusphere-2026-1016
Preprint. Discussion started: 19 March 2026

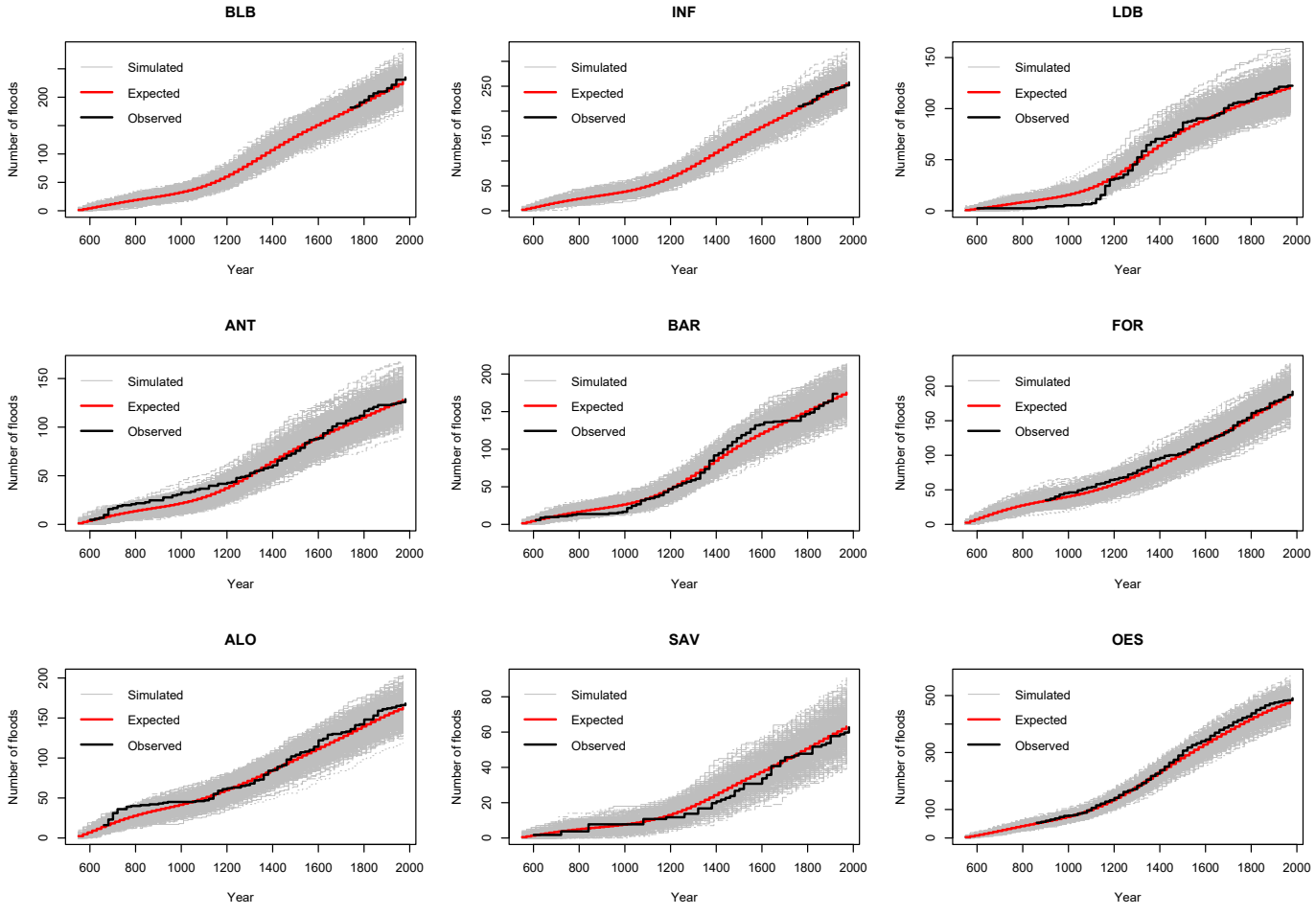

Figure A1. Comparison between in-sample simulated count processes and observed counts (1 of 3).

References

Albrecher, H., Beirlant, J., and Teugels, J. L.: Reinsurance: actuarial and statistical aspects, John Wiley & Sons, 2017.

Albrecher, H., Bladt, M., Kortschak, D., Prettenthaler, F., and Swierczynski, T.: Flood occurrence change-point analysis in the paleoflood record from Lake Mondsee (NE Alps), Global and Planetary Change, 178, 65–76, https://doi.org/10.1016/j.gloplacha.2019.04.009, 2019.

Albrecher, H., Kortschak, D., and Prettenthaler, F.: Spatial Dependence Modeling of Flood Risk Using Max-Stable Processes: The Example of Austria, Water, 12, 1805, 2020.

Bevere, L. and Remondi, F.: Natural catastrophes in 2021: the floodgates are open, Swiss Re Institute, 2022.

Blöschl, G., Gaál, L., Hall, J., Kiss, A., Komma, J., Nester, T., Parajka, J., Perdigão, R., Plavcová, L., Rogger, M., Salinas, J., and Viglione, A.: Increasing River Floods: Fiction or Reality?, WIREs Water, 2, 329–344, https://doi.org/10.1002/wat2.1079, 2015.

https://doi.org/10.5194/egusphere-2026-1016
Preprint. Discussion started: 19 March 2026

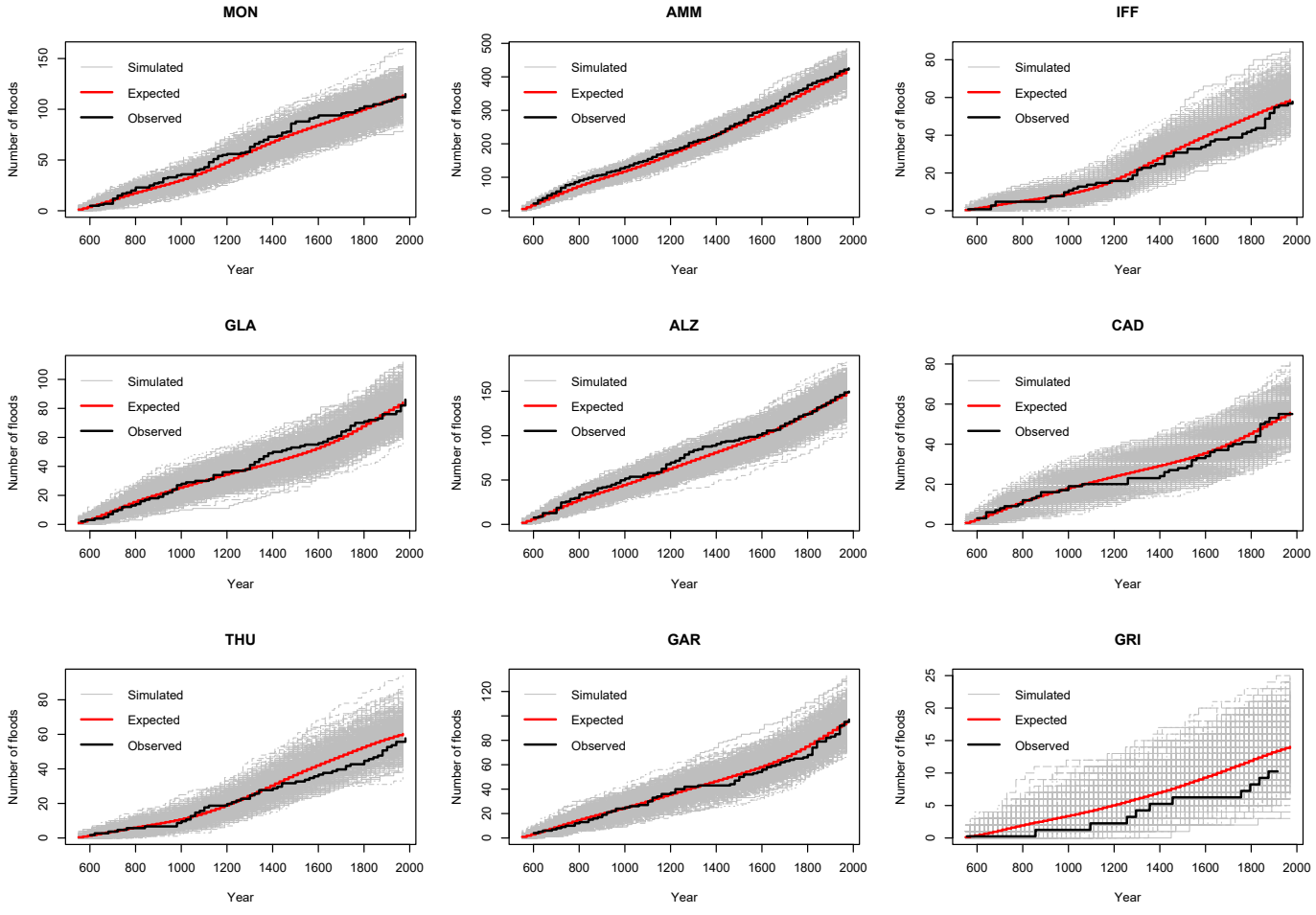

Figure A2. Comparison between in-sample simulated count processes and observed counts (2 of 3).

Blöschl, G., Hall, J., Parajka, J., Perdigão, R., Merz, B., Arheimer, B., Aronica, G., Bilibashi, A., Bonacci, O., Borga, M., Čanjevac, I., Castellarin, A., Chirico, G., Claps, P., Fiala, K., Frolova, N., Gorbachova, L., Gül, A., Hannaford, J., Harrigan, S., Kireeva, M., Kiss, A., Kjeldsen, T., Kohnová, S., Koskela, J., Ledvinka, O., Macdonald, N., Mavrova-Guirguinova, M., Mediero, L., Merz, R., Molnar, P., Montanari, A., Murphy, C., Osuch, M., Ovcharuk, V., Radevski, I., Rogger, M., Salinas, J., Sauquet, E., Šraj, M., Szolgay, J., Viglione, A., Volpi, E., Wilson, D., Zaimi, K., and Živković, N.: Changing Climate Shifts Timing of European Floods, Science, 357, 588–590, https://doi.org/10.1126/science.aan2506, 2017.

Blöschl, G., Hall, J., Viglione, A., Perdigão, R., Parajka, J., Merz, B., Lun, D., Arheimer, B., Aronica, G., Bilibashi, A., Boháč, M., Bonacci, O., Borga, M., Čanjevac, I., Castellarin, A., Chirico, G., Claps, P., Frolova, N., Ganora, D., Gorbachova, L., Gül, A., Hannaford, J., Harrigan, S., Kireeva, M., Kiss, A., Kjeldsen, T., Kohnová, S., Koskela, J., Ledvinka, O., Macdonald, N., Mavrova-Guirguinova, M., Mediero, L., Merz, R., Molnar, P., Montanari, A., Murphy, C., Osuch, M., Ovcharuk, V., Radevski, I., Salinas, J., Sauquet, E., Šraj, M.,

https://doi.org/10.5194/egusphere-2026-1016
Preprint. Discussion started: 19 March 2026

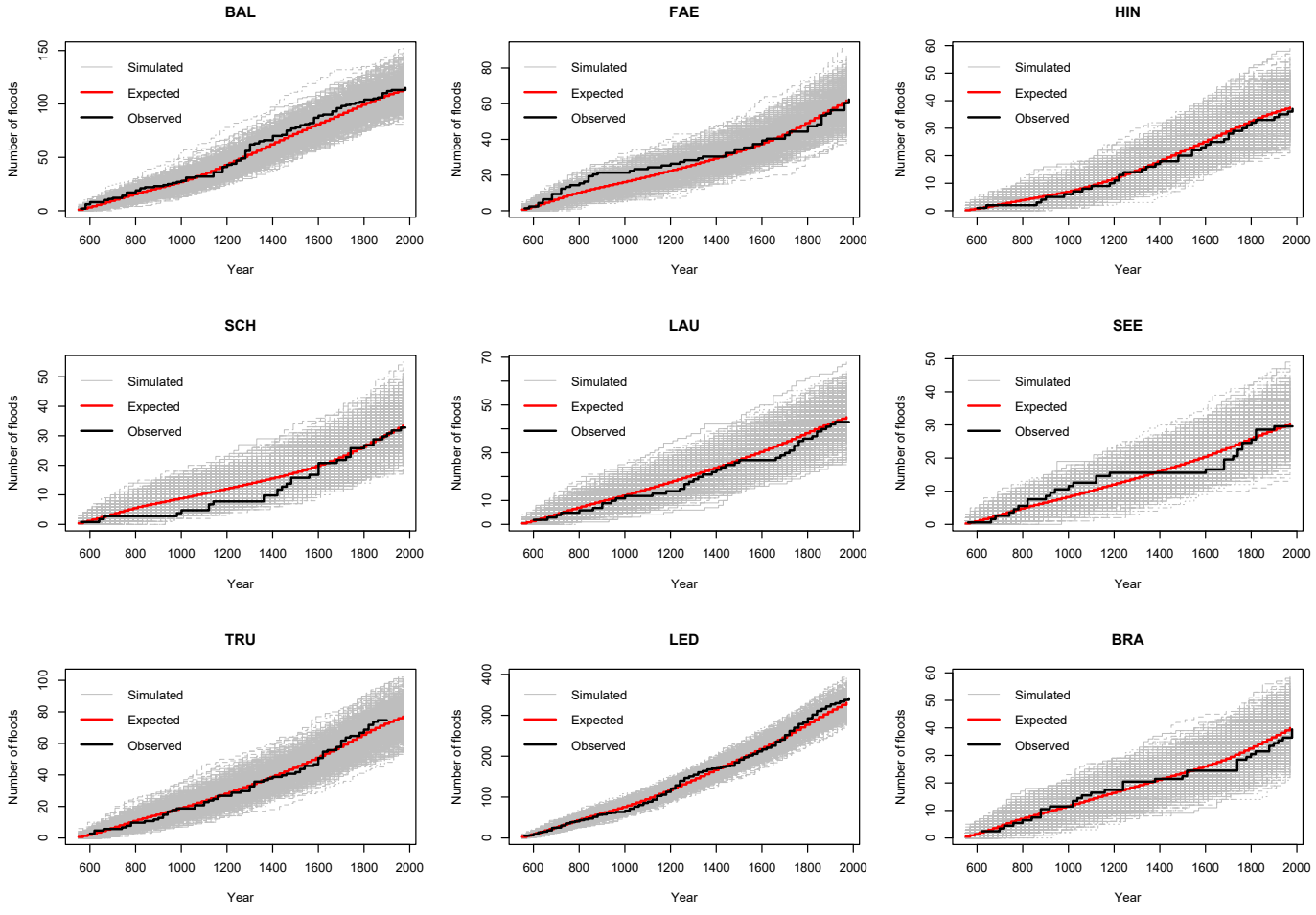

Figure A3. Comparison between in-sample simulated count processes and observed counts (3 of 3).

Szolgay, J., Volpi, E., Wilson, D., Zaimi, K., and Živković, N.: Changing climate both increases and decreases European river floods, Nature, 573, 108–111, https://doi.org/10.1038/s41586-019-1495-6, 2019.

Borgatti, L. and Soldati, M.: Landslides as a geomorphological proxy for climate change: a record from the Dolomites (northern Italy), Geomorphology, 120, 56–64, 2010.

Brázdil, R., Pfister, C., Wanner, H., Storch, H., and Luterbacher, J.: Historical Climatology In Europe – The State Of The Art, Climatic Change, 70, 363–430, https://doi.org/10.1007/s10584-005-5924-1, 2005.

Brunner, M. and Naveau, P.: Spatial Variability in Alpine Reservoir Regulation: Deriving Reservoir Operations from Streamflow Using Generalized Additive Models, Hydrology and Earth System Sciences, 27, 673–687, https://doi.org/10.5194/hess-27-673-2023, 2023.

Chebana, F., Charron, C., Ouarda, T. B. M. J., and Martel, B.: Regional Frequency Analysis at Ungauged Sites with the Generalized Additive Model, Journal of Hydrometeorology, 15, 2418 – 2428, https://doi.org/10.1175/JHM-D-14-0060.1, 2014.

https://doi.org/10.5194/egusphere-2026-1016
Preprint. Discussion started: 19 March 2026

Chiverrell, R., Sear, D., Warburton, J., Macdonald, N., Schillereff, D., Dearing, J., Croudace, I., Brown, J., and Bradley, J.: Using lake sediment archives to improve understanding of flood magnitude and frequency: Recent extreme flooding in northwest UK, Earth Surface Processes and Landforms, 44, 2366–2376, https://doi.org/10.1002/esp.4650, 2019.

Cressie, N.: Statistics for Spatial Data, Wiley Series in Probability and Statistics, John Wiley & Sons, New York, https://doi.org/10.1002/9781119115151, 1993.

Dunn, P. K. and Smyth, G. K.: Randomized Quantile Residuals, Journal of Computational and Graphical Statistics, 5, 236–244, https://doi.org/10.1080/10618600.1996.10474708, 1996.

Engeland, K., Aano, A., Steffensen, I., Støren, E., and Paasche, Ø.: New flood frequency estimates for the largest river in Norway based on the combination of short and long time series, Hydrology and Earth System Sciences, 24, 5595–5619, https://doi.org/10.5194/hess-24-5595-2020, 2020.

Gelman, A. and Hill, J.: Data Analysis Using Regression and Multilevel/Hierarchical Models, Analytical Methods for Social Research, Cambridge University Press, ISBN 9780521686891, https://books.google.ch/books?id=lV3DIdV0F9AC, 2007.

Giraldo, R., Delicado, P., and Mateu, J.: Continuous Time-Varying Kriging for Spatial Prediction of Functional Data: An Environmental Application, Journal of Agricultural, Biological, and Environmental Statistics, 15, 66–82, https://doi.org/10.1007/s13253-009-0012-z, 2010.

Glur, L., Wirth, S., Büntgen, U., Gilli, A., Haug, G., Schär, C., Beer, J., and Anselmetti, F.: Frequent floods in the European Alps coincide with cooler periods of the past 2500 years, Scientific Reports, 3, 2770, 2013.

Hartig, F.: DHARMa: Residual Diagnostics for Hierarchical (Multi-Level / Mixed) Regression Models, r package version 0.4.7, 2024.

Hastie, T. and Tibshirani, R.: Generalized Additive Models, Statistical Science, 1, 297–310, https://doi.org/10.1214/ss/1177013604, 1986.

Hijmans, R. J.: geodata: Access Geographic Data, https://doi.org/10.32614/CRAN.package.geodata, r package version 0.6-6, 2025.

Hijmans, R. J., Brown, A., and Barbosa, M.: terra: Spatial Data Analysis, https://doi.org/10.32614/CRAN.package.terra, r package version 1.9-1, 2026.

Hristopulos, D. T.: Random Fields for Spatial Data Modeling: A Primer for Scientists and Engineers, Advances in Geographic Information Science, Springer Netherlands, ISBN 978-94-024-1916-0 978-94-024-1918-4, https://doi.org/10.1007/978-94-024-1918-4, 2020.

Kochel, R. C. and Baker, V. R.: Paleoflood Hydrology, Science (New York, N.Y.), 215, 353–361, https://doi.org/10.1126/science.215.4531.353, 1982.

Massicotte, P. and South, A.: rnaturalearth: World Map Data from Natural Earth, https://doi.org/10.32614/CRAN.package.rnaturalearth, r package version 1.2.0, 2026.

Mateu, J. and Giraldo, R.: Geostatistical Functional Data Analysis, Wiley Series in Probability and Statistics, Wiley, 2021.

Merz, B., Nguyen, V., and Vorogushyn, S.: Temporal clustering of floods in Germany: Do flood-rich and flood-poor periods exist?, Journal of Hydrology, 541, 824–838, https://doi.org/10.1016/j.jhydrol.2016.07.041, 2016.

Mudelsee, M., Börngen, M., Tetzlaff, G., and Grünewald, U.: No upward trends in the occurrence of extreme floods in central Europe, Nature, 425, 166–169, https://doi.org/10.1038/nature01928, 2003.

PAGES – Past Global Changes: Floods Working Group, https://pastglobalchanges.org/science/wg/floods/intro, accessed 1 July 2025, 2025.

Pebesma, E.: Multivariable geostatistics in S: the gstat package, Computers & Geosciences, 30, 683–691, https://doi.org/https://doi.org/10.1016/j.cageo.2004.03.012, 2004.

https://doi.org/10.5194/egusphere-2026-1016
Preprint. Discussion started: 19 March 2026

Rahman, A., Charron, C., Ouarda, T. B. M. J., and Chebana, F.: Development of Regional Flood Frequency Analysis Techniques Using Generalized Additive Models for Australia, Stochastic Environmental Research and Risk Assessment, 32, 123–139, https://doi.org/10.1007/s00477-017-1384-1, 2018.

Rima, L., Haddad, K., and Rahman, A.: Generalised Additive Model-Based Regional Flood Frequency Analysis: Parameter Regression Technique Using Generalised Extreme Value Distribution, Water, 17, 206, https://doi.org/10.3390/w17020206, 2025.

Ruiz-Villanueva, V. and Molnar, P.: Past, Current, and Future Changes in Floods in Switzerland, Report, ETH Zurich, https://doi.org/10.3929/ethz-b-000458556, 2020.

Schmocker-Fackel, P. and Naef, F.: Changes in Flood Frequencies in Switzerland since 1500, Hydrology and Earth System Sciences, 14, 1581–1594, https://doi.org/10.5194/hess-14-1581-2010, 2010.

Schröer, G. and Trenkler, D.: Exact and randomization distributions of Kolmogorov-Smirnov tests two or three samples, Computational Statistics & Data Analysis, 20, 185–202, https://doi.org/https://doi.org/10.1016/0167-9473(94)00040-P, 1995.

Selch, D. A., Scherer, M., et al.: A multivariate claim count model for applications in insurance, Springer, 2018.

Swierczynski, T., Lauterbach, S., Dulski, P., Delgado, J., Merz, B., and Brauer, A.: Mid- to late Holocene flood frequency changes in the northeastern Alps as recorded in varved sediments of Lake Mondsee (Upper Austria), Quaternary Science Reviews, 80, 78–90, https://doi.org/10.1016/j.quascirev.2013.08.018, 2013.

Tinner, W. and Ammann, B.: Timberline paleoecology in the Alps, Pages News, 9, 9–11, 2001.

Waltgenbach, S., Scholz, D., Spötl, C., Riechelmann, D., Jochum, K., Fohlmeister, J., and Schröder-Ritzrau, A.: Climate and structure of the 8.2 ka event reconstructed from three speleothems from Germany, Global and Planetary Change, 193, 103 266, 2020.

Wilhelm, B., Ballesteros Cánovas, J., Macdonald, N., Toonen, W., Baker, V., Barriendos, M., Benito, G., Brauer, A., Corella, J., Denniston, R., Glaser, R., Ionita, M., Kahle, M., Liu, T., Luetscher, M., Macklin, M., Mudelsee, M., Munoz, S., Schulte, L., St. George, S., Stoffel, M., and Wetter, O.: Interpreting historical, botanical, and geological evidence to aid preparations for future floods, WIREs Water, 6, e1318, https://doi.org/10.1002/wat2.1318, 2019.

Wilhelm, B., Rapuc, W., Amann, B., Anselmetti, F. S., Arnaud, F., Blanchet, J., Brauer, A., Czymzik, M., Giguet-Covex, C., Gilli, A., Glur, L., Grosjean, M., Irmler, R., Nicolle, M., Sabatier, P., Swierczynski, T., and Wirth, S. B.: Impact of warmer climate periods on flood hazard in the European Alps, Nature Geoscience, 15, 118–123, https://doi.org/10.1038/s41561-021-00878-y, 2022.

Wood, S.: Low-Rank Scale-Invariant Tensor Product Smooths for Generalized Additive Mixed Models, Biometrics, 62, 1025–1036, https://doi.org/10.1111/j.1541-0420.2006.00574.x, 2006.

Wood, S.: Fast Stable Restricted Maximum Likelihood and Marginal Likelihood Estimation of Semiparametric Generalized Linear Models, Journal of the Royal Statistical Society Series B: Statistical Methodology, 73, 3–36, https://doi.org/10.1111/j.1467-9868.2010.00749.x, 2010.

Wood, S.: Generalized Additive Models: An Introduction with R, Second Edition, Chapman and Hall/CRC, 2 edn., https://doi.org/10.1201/9781315370279, 2017.

Wood, S. and Wood, M. S.: Package 'mgcv', R package version, 1, 729, 2015.

Wood, S. N., Bravington, M. V., and Hedley, S. L.: Soap Film Smoothing, Journal of the Royal Statistical Society: Series B (Statistical Methodology), 70, 931–955, https://doi.org/10.1111/j.1467-9868.2008.00665.x, 2008.